

See discussions, stats, and author profiles for this publication at: <https://www.researchgate.net/publication/229063453>

Spectroscopic and Electrochemical Study of the Interconversion and Decomplexation of Cobalt(II) Sandwich Polyoxometalates Based on a Dawson-Type Anion

ARTICLE *in* INORGANIC CHEMISTRY · JULY 2012

Impact Factor: 4.76 · DOI: 10.1021/ic3007603 · Source: PubMed

CITATIONS

7

READS

16

6 AUTHORS, INCLUDING:



Laurent Ruhlmann

University of Strasbourg

79 PUBLICATIONS 1,254 CITATIONS

[SEE PROFILE](#)



Delphine Schaming

33 PUBLICATIONS 349 CITATIONS

[SEE PROFILE](#)

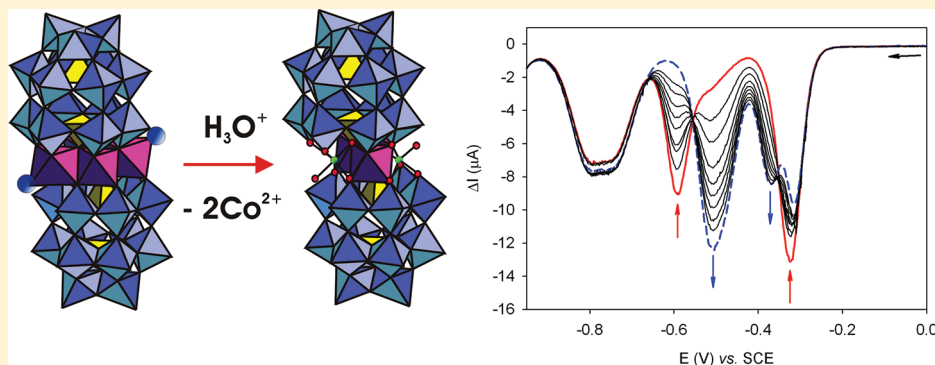
Spectroscopic and Electrochemical Study of the Interconversion and Decomplexation of Cobalt(II) Sandwich Polyoxometalates Based on a Dawson-Type Anion

Laurent Ruhlmann,^{*,†,‡} Delphine Schaming,[†] Iftikhar Ahmed,^{†,‡} Aimeric Courville,[†] Jacqueline Canny,[§] and René Thouvenot^{*,§}

[†]Laboratoire de Chimie Physique (UMR CNRS 8000), Bâtiment 349, Université de Paris-Sud 11, 91405 Orsay Cedex, France

[‡]Laboratoire d'Electrochimie et de Chimie-Physique du Corps Solide (UMR CNRS 7177), Université de Strasbourg, 4 rue Blaise Pascal, 67081 Strasbourg, France

[§]Institut Parisien de Chimie Moléculaire (UMR CNRS 7201), Case courrier 42, Université Pierre et Marie Curie Univ Paris 06, 4 Place Jussieu, 75252 Paris Cedex, France



ABSTRACT: The reaction of the trivacant Dawson polyoxometalate $\alpha\text{-}[\text{P}_2\text{W}_{15}\text{O}_{56}]^{12-}$ and the divalent cations Co^{2+} is known to form a symmetrically derived sandwich complex of formula $\beta\beta\text{-}[\text{Co}_4(\text{H}_2\text{O})_2(\text{P}_2\text{W}_{15}\text{O}_{56})_2]^{16-}$ [symbolized as $\beta\beta\text{-Co}_4(\text{P}_2\text{W}_{15})_2$] at low pH (ca. pH 3). We have shown previously that, by a slight modification of the reaction conditions, trinuclear $\alpha\beta\text{-}[(\text{NaOH}_2)\text{Co}_3(\text{H}_2\text{O})(\text{P}_2\text{W}_{15}\text{O}_{56})_2]^{17-}$ and dinuclear $[(\text{NaOH}_2)_2\text{Co}_2(\text{P}_2\text{W}_{15}\text{O}_{56})_2]^{18-}$ complexes [symbolized as $\alpha\beta\text{-NaCo}_3(\text{P}_2\text{W}_{15})_2$ and $\text{Na}_2\text{Co}_2(\text{P}_2\text{W}_{15})_2$, respectively] can be synthesized as aqueous-soluble sodium salts. $\alpha\beta\text{-NaCo}_3(\text{P}_2\text{W}_{15})_2$ is a “lacunary” sandwich complex that can add a Co^{2+} cation according to $\alpha\beta\text{-NaCo}_3(\text{P}_2\text{W}_{15})_2 + \text{Co}^{2+} \rightarrow \alpha\beta\text{-Co}_4(\text{P}_2\text{W}_{15})_2 + \text{Na}^+$ to form nearly quantitatively an unsymmetrical Dawson tetracobalt sandwich polyoxometalate, $\alpha\beta\text{-}[\text{Co}_4(\text{H}_2\text{O})_2(\text{P}_2\text{W}_{15}\text{O}_{56})_2]^{16-}$ [symbolized as $\alpha\beta\text{-Co}_4(\text{P}_2\text{W}_{15})_2$]. Thus, for $\text{Co}_4(\text{P}_2\text{W}_{15})_2$, the junctions between the trivacant $\{\text{P}_2\text{W}_{15}\}$ subunits and the central tetrameric unit can be either β type or both β and α types. The interconversion between $\alpha\beta\text{-Co}_4(\text{P}_2\text{W}_{15})_2$ and $\beta\beta\text{-Co}_4(\text{P}_2\text{W}_{15})_2$ and the decomplexation process at low pH, leading to the formation of $\alpha\beta\text{-NaCo}_3(\text{P}_2\text{W}_{15})_2$ and/or $\text{Na}_2\text{Co}_2(\text{P}_2\text{W}_{15})_2$, have been followed in aqueous solution at various pH values by electrochemistry, UV-visible absorption spectroscopy, and ^{31}P NMR spectroscopy.

INTRODUCTION

In general, polyoxometalate anions exhibit varied structures, rich redox chemistry, photochemistry, and an ability to catalyze a wide range of industrially and biologically significant reactions.¹

The applications of polyoxometalates are based on their unique properties, including size, electron- and proton-transfer/storage abilities, thermal stability, lability of the lattice oxygen, and high Brønsted acidity of the corresponding acids.²

In medicinal chemistry, polyoxometalates exhibit biological activity, such as highly selective inhibition of enzymes and in vitro and in vivo antitumoral, antiviral, and antiretroviral activities.³

Polyoxometalate compounds provide a good basis for the molecular design of mixed oxide catalysts, and they have high capability in practical uses. The catalytic function of polyoxometalate compounds is used in solution as well as in the solid state, as acid⁴ and reduction^{5,6} catalysts. The research activity in the field of polyoxometalates is very high and still growing.

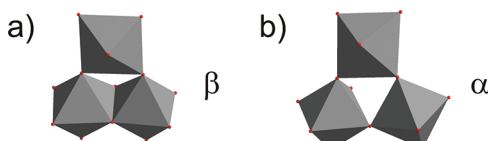
Since the first report by Finke and Droege in 1983,⁷ the synthesis of sandwich polyoxometalates derived from the trivacant anion $\alpha\text{-}[\text{P}_2\text{W}_{15}\text{O}_{56}]^{12-}$ (abbreviated as P_2W_{15}) has received increased attention because of their physicochemical

Received: April 13, 2012

and catalytical properties.^{4–6} These compounds result from the reaction of the trivacant anion $\alpha\text{-}\left[\text{P}_2\text{W}_{15}\text{O}_{56}\right]^{12-}$ with transition-metal cations ($\text{M} = \text{Mn}^{\text{II}}, \text{Fe}^{\text{III}}, \text{Co}^{\text{II}}, \text{Ni}^{\text{II}}, \text{Cu}^{\text{II}}, \text{Zn}^{\text{II}}$, and Cd^{II}). When a sheet of four M atoms is sandwiched between two $\{\text{P}_2\text{W}_{15}\}$ subunits, complexes of the formula $[\text{M}_4(\text{H}_2\text{O})_2(\text{P}_2\text{W}_{15}\text{O}_{56})_2]^{n-}$ are obtained.⁸ Such complexes can be considered as “saturated” because they possess the maximum number of d metal centers that can be sandwiched by two trivacant anions $\{\text{P}_2\text{W}_{15}\}$.

For all known Dawson tetranuclear sandwich complexes characterized by X-ray diffraction, the “classical” $\beta\beta$ configuration is observed with β connectivities between both trivacant $\{\text{P}_2\text{W}_{15}\}$ units and the central M_4 tetrad (Scheme 1a).^{8b,d,e,g,k}

Scheme 1. Representations of the (a) β and (b) α Junctions



Let us remind the reader that the β junction implies a connection between one WO_6 and a dimetallic unit W_2O_{10} , whereas the α junction is defined as a bis(μ -oxo) connection between two dimeric units W_2O_{10} (Scheme 1); alternately, the α junction may be described by a group of three mutually corner-coupled WO_6 octahedra.⁹

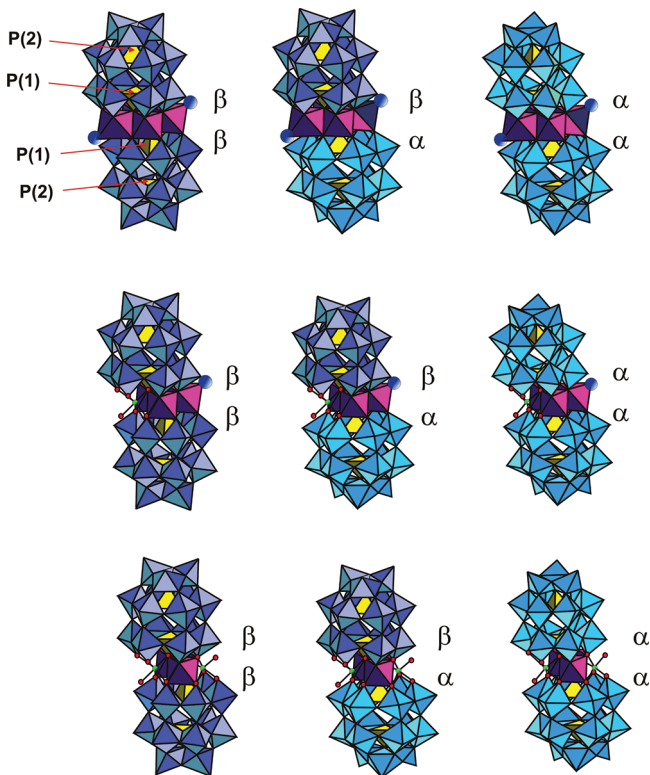
Nevertheless, in the case of the tetracobalt sandwich complexes, we have reported that in neutral medium a mixture of $\beta\beta$ and $\alpha\beta$ configurations has been observed.¹⁹

Dinuclear and trinuclear sandwich complexes $[(\text{NaOH}_2)_2\text{M}_2(\text{P}_2\text{W}_{15}\text{O}_{56})_2]^{n-}$ and $[(\text{NaOH}_2)\text{M}_3(\text{H}_2\text{O})-(\text{P}_2\text{W}_{15}\text{O}_{56})_2]^{n-}$ ($\text{M} = \text{Co}^{\text{II}}, \text{Mn}^{\text{II}}, \text{Ni}^{\text{II}}$, and Fe^{III})^{10–14} were also obtained (Scheme 2). The first example of a sandwich-type species with less than four d metals was reported by Hill et al.¹² X-ray structures of the di- and triiron derivatives as well as of the trimanganese and tricobalt derivatives have been reported.^{11–13} For the diiron sandwich $[(\text{NaOH}_2)_2\text{Fe}_2(\text{P}_2\text{W}_{15}\text{O}_{56})_2]^{16-}$ [symbolized as $\text{Na}_2\text{Fe}_2(\text{P}_2\text{W}_{15})_2$], the junctions between the trivacant units $\{\text{P}_2\text{W}_{15}\}$ and the metallic sheet are both of α type (Scheme 2), whereas in the case of the triiron complex, the structure may be considered as resulting from the fusion of one $\alpha\text{-}\{\text{Fe}_3(\text{P}_2\text{W}_{15})\}$ unit and one “lacunary” $\beta\text{-}\{\text{NaFe}_2(\text{P}_2\text{W}_{15})\}$ unit, where the central sheet consists of three d metals and one labile Na^+ cation.

A similar $\alpha\beta$ connectivity has been reported for tricobalt species $[(\text{NaOH}_2)\text{Co}_3(\text{H}_2\text{O})(\text{P}_2\text{W}_{15}\text{O}_{56})_2]^{17-}$ [abbreviated as $\text{NaCo}_3(\text{P}_2\text{W}_{15})_2$; Scheme 2];^{10,11} in contrast, the trimanganese derivative exhibits a $\beta\beta$ connectivity for both trivacant moieties $\{\text{P}_2\text{W}_{15}\}$.¹³ This suggests that the nature and number of transition-metal cations in the central sheet as well as the conditions of the synthesis play an important role for the type of connectivity.¹⁵ Moreover, the pH, the ratio of transition-metal cation to trivacant moieties, the concentration, and the ionic strength also play crucial roles in the preparation of pure compounds.

Because the Na^+ cations are weakly bonded and labile, $[(\text{NaOH}_2)_2\text{M}_2(\text{P}_2\text{W}_{15}\text{O}_{56})_2]^{n-}$ and $[(\text{NaOH}_2)\text{M}_3(\text{H}_2\text{O})-(\text{P}_2\text{W}_{15}\text{O}_{56})_2]^{n-}$ complexes may act as a divacant and monovacant lacunary species, respectively. Thus, mixed-metal sandwich complexes can be obtained easily by the reaction of a

Scheme 2. Structural Relationship between the Different Cobalt Sandwich Complex Isomers Based on $\alpha\text{-}\left[\text{P}_2\text{W}_{15}\text{O}_{56}\right]^{12-}$: $\text{Co}_4(\text{P}_2\text{W}_{15})_2$ (Top); $\text{NaCo}_3(\text{P}_2\text{W}_{15})_2$ (Center); $\text{Na}_2\text{Co}_2(\text{P}_2\text{W}_{15})_2$ (Bottom)



transition-metal cation M^{m+} with $\text{Na}_2\text{Fe}_2(\text{P}_2\text{W}_{15})_2$. Indeed, it was shown that $\alpha\alpha\text{-}\text{Na}_2\text{Fe}_2(\text{P}_2\text{W}_{15})_2$ reacts with M^{2+} ($\text{M} = \text{Mn}, \text{Co}, \text{Ni}, \text{Zn}$), leading to a “saturated” mixed-metal sandwich-type polyanion $[\text{M}^{\text{II}}_2(\text{H}_2\text{O})_2\text{Fe}^{\text{III}}_2(\text{P}_2\text{W}_{15}\text{O}_{56})_2]^{14-}$ [abbreviated as $\text{M}_2\text{Fe}_2(\text{P}_2\text{W}_{15})_2$].^{12,16,17} Two M^{2+} replace the two Na^+ ions of $\text{Na}_2\text{Fe}_2(\text{P}_2\text{W}_{15})_2$ with the simultaneous rearrangement of the whole structure back to the conventional inter-POM-unit connectivity $\beta\beta$ junction. At relatively high pH (ca. 5–6), $\alpha\alpha\text{-}\text{Na}_2\text{Fe}_2(\text{P}_2\text{W}_{15})_2$ incorporates only one transition-metal cation M ($\text{M} = \text{Fe}^{3+}, \text{Co}^{2+}, \text{Cu}^{2+}$) into the central sheet to yield a still “lacunary” sandwich species, with one α junction and one β junction between the trivacant $\{\text{P}_2\text{W}_{15}\}$ subunits and the $\{\text{NaMFe}_2\}$ unit.^{12b}

Similarly, the “lacunary” sandwich complex $\alpha\beta\text{-}\text{Na}_2\text{Co}_3(\text{P}_2\text{W}_{15})_2$ can add one Co^{2+} cation to form nearly quantitatively an unsymmetrical tetracobalt sandwich complex $\alpha\beta\text{-}[\text{Co}_4(\text{H}_2\text{O})(\text{P}_2\text{W}_{15}\text{O}_{56})_2]^{16-}$ [symbolized as $\alpha\beta\text{-}\text{Co}_4(\text{P}_2\text{W}_{15})_2$].¹⁸ This synthesis proceeds in a relatively narrow pH range (5–6 > pH > 3.5) and high reactant concentrations; using different conditions leads to a mixture of various complexes.

Herein we report the study of the interconversion between $\alpha\beta\text{-}\text{Co}_4(\text{P}_2\text{W}_{15})_2$ and $\beta\beta\text{-}\text{Co}_4(\text{P}_2\text{W}_{15})_2$ as well as the decomposition process at low pH, leading to the formation of $\alpha\beta\text{-}\text{NaCo}_3(\text{P}_2\text{W}_{15})_2$ and $\alpha\beta\text{-}\text{Na}_2\text{Co}_2(\text{P}_2\text{W}_{15})_2$. This system was investigated under various conditions (pH and concentration) by electrochemistry, UV-visible absorption spectroscopy, and ^{31}P NMR spectroscopy.

129 ■ RESULTS AND DISCUSSION

130 **Preliminary Considerations.** All syntheses were per-
131 formed starting from $\alpha\text{-}[\text{P}_2\text{W}_{15}\text{O}_{56}]^{12-}$ prepared from pure $\alpha\text{-}$
132 $[\text{P}_2\text{W}_{18}\text{O}_{62}]^{6-}$.

133 We previously reported the synthesis of the $\text{Co}_4(\text{P}_2\text{W}_{15})_2$
134 species from Co^{2+} and $\alpha\text{-}[\text{P}_2\text{W}_{15}\text{O}_{56}]^{12-}$.¹⁹ The ^{31}P NMR
135 spectrum of the compound obtained via synthesis in a neutral
136 medium indicated the presence of a mixture of the symmetrical
137 $\beta\beta\text{-Co}_4(\text{P}_2\text{W}_{15})_2$ ($\delta = +1459$ and $+9.8$ ppm) and unsymmetrical
138 $\alpha\beta\text{-Co}_4(\text{P}_2\text{W}_{15})_2$ ($\delta = +1551$, $+1242$, $+16.7$, and $+12.3$ ppm)
139 complexes in relative proportions 38 and 62% (by integration
140 of the NMR resonances).^{19,20} Unfortunately, the solubilities of
141 these two compounds are very close, which precludes their
142 separation by selective precipitation or crystallization. Thus, a
143 neutral medium is not an optimal condition for the synthesis of
144 $\beta\beta\text{-Co}_4(\text{P}_2\text{W}_{15})_2$.

145 On the contrary, optimal conditions for the synthesis of the
146 symmetrical $\beta\beta\text{-Co}_4(\text{P}_2\text{W}_{15})_2$, from Co^{2+} and $\alpha\text{-}[\text{P}_2\text{W}_{15}\text{O}_{56}]^{12-}$,
147 required an acidic medium (pH ~ 3).¹⁹ Indeed, in contrast to a
148 neutral medium, synthesis in an acidic solution (pH ≈ 3) gives
149 exclusively the symmetrical $\beta\beta\text{-Co}_4(\text{P}_2\text{W}_{15})_2$ species with a
150 purity of 95%.

151 Concerning the unsymmetrical species $\alpha\beta\text{-Co}_4(\text{P}_2\text{W}_{15})_2$, the
152 best method of synthesis consists of starting from the sandwich
153 complex $\alpha\beta\text{-NaCo}_3(\text{P}_2\text{W}_{15})_2$.¹⁸ This synthesis requires a neutral
154 medium, i.e., pH 6.5. The formation of the “saturated”
155 tetracobalt species $\alpha\beta\text{-Co}_4(\text{P}_2\text{W}_{15})_2$ was followed by ^{31}P
156 NMR in solution. The ^{31}P NMR solution spectrum of the
157 starting compound $\alpha\beta\text{-NaCo}_3(\text{P}_2\text{W}_{15})_2$ presents two narrow
158 lines [$\Delta\nu_{1/2} = 10$ Hz, P(2) farthest from the tricobalt central
159 cluster] of equal intensity, at $\delta = -9.3$ and $+22.0$ ppm, and two
160 broad bands ($\Delta\nu_{1/2} = 450$ Hz) at $\delta = +1125$ and $+1673$ ppm
161 [P(1) nuclei close to the tricobalt central cluster; see Table 1].

Table 1. ^{31}P NMR Data for the Cobalt Sandwich Species Obtained from Pure Compounds^a

compound	P(1) ^b		P(2) ^b	
	δ^c	$\Delta\nu_{1/2}^d$	δ^c	$\Delta\nu_{1/2}^d$
$\beta\beta\text{-Co}_4(\text{P}_2\text{W}_{15})_2$	+1483	420	+9.9	20
$\alpha\beta\text{-Co}_4(\text{P}_2\text{W}_{15})_2$	+1203	420	+10.0	20
	+1522	420	+14.5	20
$\alpha\beta\text{-NaCo}_3(\text{P}_2\text{W}_{15})_2$	+1125	450	-9.3	10
	+1673	450	+22.0	10
$\text{Na}_2\text{Co}_2(\text{P}_2\text{W}_{15})_2$	+1299	300	+4.2	10

^aA 0.02 mol L⁻¹ unbuffered solution in D₂O/H₂O (1:1) measured at 300 K. ^bP(1) and P(2) in the PW₆ and PW₉ subunits, respectively. ^cIn ppm with respect to 85% H₃PO₄. ^dIn Hz.

162 The addition of Co^{2+} to the aqueous solution of $\alpha\beta\text{-}$
163 $\text{NaCo}_3(\text{P}_2\text{W}_{15})_2$ (pH 6.5) induces the appearance of new
164 signals in the ^{31}P NMR spectrum, namely, two narrow lines
165 ($\Delta\nu_{1/2} = 20$ Hz) at $\delta = +10.0$ and $+14.5$ ppm [P(2)] and two
166 broad bands ($\Delta\nu_{1/2} = 420$ Hz) at $\delta = +1203$ and $+1522$ ppm
167 [P(1); see Table 1], corresponding to the saturated tetracobalt
168 species $\alpha\beta\text{-Co}_4(\text{P}_2\text{W}_{15})_2$.

169 A total of 1 equiv of Co^{2+} per $\alpha\beta\text{-NaCo}_3(\text{P}_2\text{W}_{15})_2$ should be
170 sufficient to convert it quantitatively to $\alpha\beta\text{-Co}_4(\text{P}_2\text{W}_{15})_2$.
171 However, for synthetic purposes, in order to obtain the highest
172 yield of $\alpha\beta\text{-Co}_4(\text{P}_2\text{W}_{15})_2$, we have processed with a 2-fold
173 excess (2 equiv) of Co^{2+} with respect to the reaction
174 stoichiometry.

175 **Study of the $\alpha\beta\text{-}\beta\beta$ Interconversion for $\text{Co}_4(\text{P}_2\text{W}_{15})_2$.** After the addition of 2 equiv of H₃O⁺ (pH ca. 1.70),
176 in an unbuffered medium, to the solution containing the
177 dissymmetrical $\alpha\beta\text{-Co}_4(\text{P}_2\text{W}_{15})_2$ ($c = 0.02$ mol L⁻¹), it evolves
178 slowly into its symmetrical $\beta\beta$ isomer. The pH of the solution
179 evolves also slightly, with the final pH being 2.5.
180

181 A preliminary study of the reaction was conducted by ^{31}P
182 NMR spectroscopy: the region of P(2) shows the vanishing of
183 signals at +14.5 and +10.0 ppm^{18,19} attributed to the
184 dissymmetrical complex $\alpha\beta\text{-Co}_4(\text{P}_2\text{W}_{15})_2$ and the formation
185 of one transient species, which has been identified as $\alpha\beta\text{-}$
186 $\text{NaCo}_3(\text{P}_2\text{W}_{15})_2$ (black circle symbols in Figure 1b).
187

188 Analysis of these data implies the following successive
189 reactions: (i) decomplexation of the dissymmetrical $\alpha\beta\text{-}$
190 $\text{Co}_4(\text{P}_2\text{W}_{15})_2$ compound to form the monolacunary $\alpha\beta\text{-}$
191 $\text{NaCo}_3(\text{P}_2\text{W}_{15})_2$, (ii) isomerization of $\alpha\beta\text{-NaCo}_3(\text{P}_2\text{W}_{15})_2$ by
192 the formal rotation of a whole $\alpha\text{-P}_2\text{W}_{15}$ subunit, leading to both
193 β -type junctions at the NaCo₃ tetrad, and finally (iii) recomplexation
194 with Co^{2+} (dotted square part, Scheme 3).
195

196 The second step, which implies a structural rearrangement, is
197 likely a slow process, whereas recomplexation of Co^{2+} is likely
198 relatively rapid. These may explain why the concentration of
199 $\beta\beta\text{-NaCo}_3\text{P}_4\text{W}_{30}$ remains too low to be observed by ^{31}P NMR
200 spectroscopy.
201

202 Additional experiments show that the reaction is complete
203 only with 2 equiv of H₃O⁺ per sandwich complex; thus, pure
204 $\beta\beta\text{-Co}_4(\text{P}_2\text{W}_{15})_2$ is obtained after 90 min (Figure 1c).
205

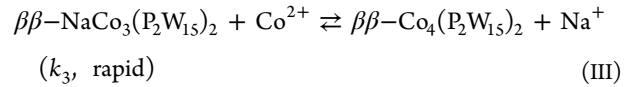
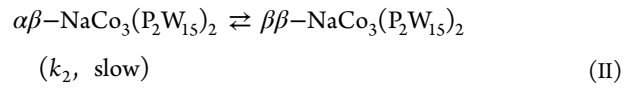
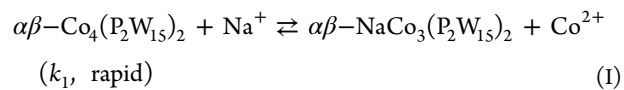
206 In order to follow more easily the interconversion process,
207 the study was performed in a buffered solution at higher pH
208 (pH 3.0). Indeed, the pH increase leads to a slowdown of the
209 kinetics of the reactions.
210

211 The detailed study was conducted by ^{31}P NMR spectroscopy
212 using $\alpha\beta\text{-Co}_4(\text{P}_2\text{W}_{15})_2$ ($c = 0.02$ mol L⁻¹) in D₂O/H₂O (1:1)
213 in 0.5 mol L⁻¹ Na₂SO₄ + H₂SO₄ at pH 3.0 (Figure 2).
214

215 The ^{31}P NMR spectra were recorded only in the low-
216 frequency region (from -15 to +25 ppm), i.e., for P(2) nuclei
217 far from the paramagnetic centers. The relative concentrations
218 of the different species are obtained by integration of the ^{31}P
219 NMR signals.
220

221 It should be noticed that, immediately (i.e. ca. 3 min) after
222 preparation of the solution, already 46% of $\alpha\beta\text{-Co}_4(\text{P}_2\text{W}_{15})_2$
223 disappeared, leading to unsaturated $\alpha\beta\text{-NaCo}_3(\text{P}_2\text{W}_{15})_2$ (+22.4
224 and -7.5 ppm) and saturated $\beta\beta\text{-Co}_4(\text{P}_2\text{W}_{15})_2$ (ca. 38% and
225 8%, respectively). The concentrations of $\alpha\beta\text{-Co}_4(\text{P}_2\text{W}_{15})_2$ and
226 $\alpha\beta\text{-NaCo}_3(\text{P}_2\text{W}_{15})_2$ decrease with time for the benefit of the
227 symmetrical complex $\beta\beta\text{-Co}_4(\text{P}_2\text{W}_{15})_2$ (signal at +7.6
228 ppm).
229

230 In accordance with the assumption proposed before, the
231 present results may also be analyzed as follows:
232



233 The first step leading to the formation of $\alpha\beta\text{-NaCo}_3(\text{P}_2\text{W}_{15})_2$ is
234 very fast. The second step implies important structural
235 rearrangement, which is consistent with the slowness of this
236

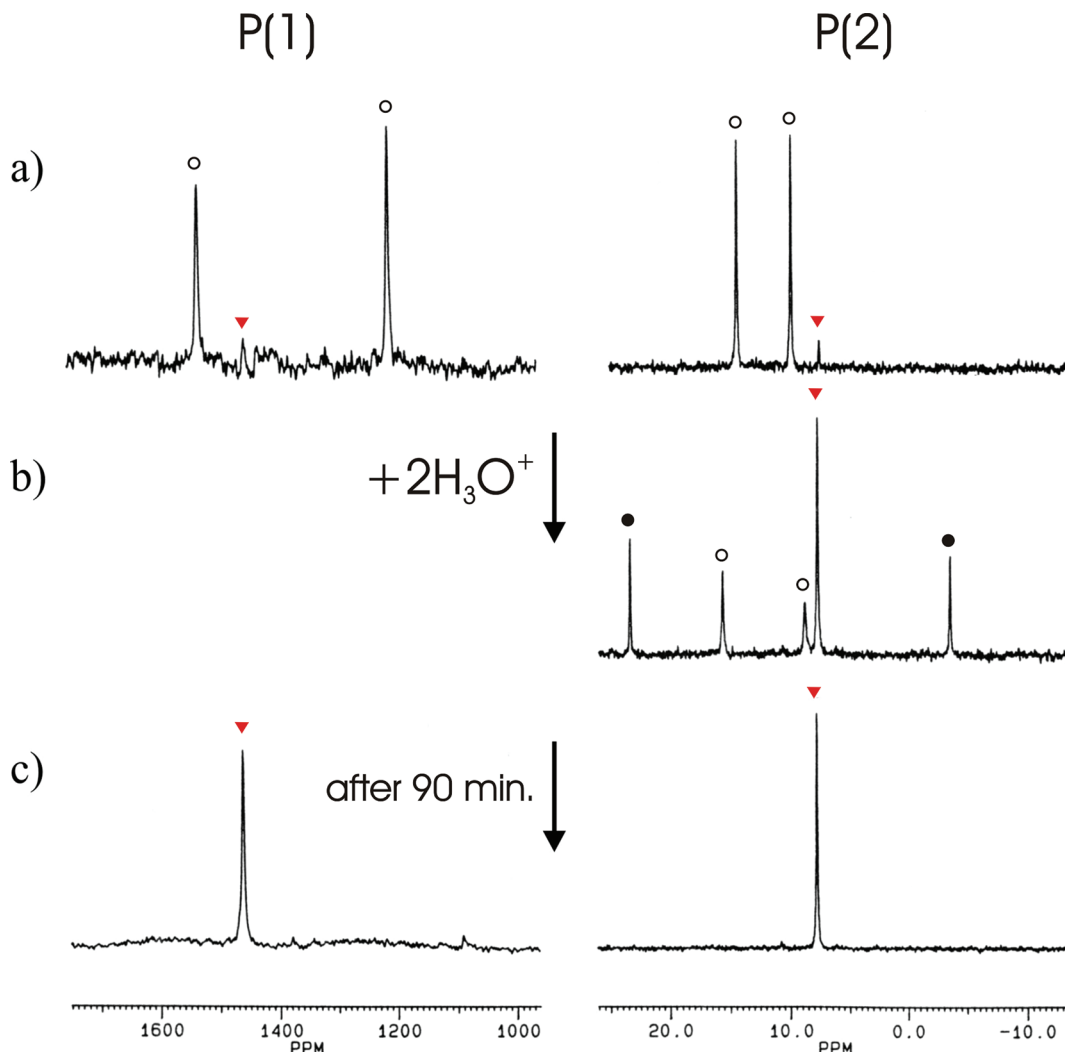


Figure 1. 121.5 MHz ^{31}P NMR study of the reactivity of (a) $\alpha\beta\text{-Co}_4(\text{P}_2\text{W}_{15})_2$ as the initial spectrum, (b) immediately after the addition of 2 equiv of H_3O^+ [the P(1) region is not given because the acquisition needs several minutes to be achieved], and (c) after 90 min with $c = 2 \times 10^{-2} \text{ mol L}^{-1}$ in $\text{D}_2\text{O}/\text{H}_2\text{O}$ (1:1) and pH ca. 1.7: (\blacktriangledown) symmetrical $\beta\beta\text{-Co}_4(\text{P}_2\text{W}_{15})_2$; (\circ) unsymmetrical $\alpha\beta\text{-Co}_4(\text{P}_2\text{W}_{15})_2$; (\bullet) $\alpha\beta\text{-NaCo}_3(\text{P}_2\text{W}_{15})_2$. Left part: region of the P(1) atoms. Experimental conditions: spectral width 125 kHz; pulse width 2 μs (ca. 40° flip angle); 8K data points; acquisition time 33 ms; ca. 10000 transients acquired without relaxation delay; line broadening factor 40 Hz. Right part: region of the P(2) atoms. Experimental conditions: spectral width 9 kHz; pulse width 2 μs (ca. 40° flip angle); 4K data points; acquisition time 0.23 s; ca. 1000 transients acquired without relaxation delay; line broadening factor 4 Hz.

process, whereas complexation of transient species with Co^{2+} remains always relatively rapid. Isomer $\beta\beta\text{-NaCo}_3(\text{P}_2\text{W}_{15})_2$ is still not observed, which suggests that the last equilibrium proceeds without a significant concentration of the intermediate species and, consequently, that reaction (III) is more rapid than reaction (II) ($k_3 \gg k_2$).

Effect of the pH on the $\alpha\beta\text{-}\beta\beta$ Interconversion. We have already shown by ^{31}P NMR (Figure 3), electrochemistry, and UV-visible absorption spectroscopy that, at pH > 3.5 and in high concentration ($\geq 2 \times 10^{-2} \text{ mol L}^{-1}$), $\alpha\beta\text{-Co}_4(\text{P}_2\text{W}_{15})_2$, $\beta\beta\text{-Co}_4(\text{P}_2\text{W}_{15})_2$, and $\alpha\beta\text{-NaCo}_3(\text{P}_2\text{W}_{15})_2$ are stable for at least 1 month.^{10,18} Only in the case of $\text{Na}_2\text{Co}_2(\text{P}_2\text{W}_{15})_2$ has isomerization been observed.¹⁰

We have also shown earlier that, at the same concentration ($2 \times 10^{-2} \text{ mol L}^{-1}$) but at lower pH ($2.5 < \text{pH} < 3.5$), $\alpha\beta\text{-Co}_4(\text{P}_2\text{W}_{15})_2$ isomerizes to $\beta\beta\text{-Co}_4(\text{P}_2\text{W}_{15})_2$ through formation of the transient $\alpha\beta\text{-NaCo}_3(\text{P}_2\text{W}_{15})_2$ species (Figure 4A).

Finally, in a more acidic solution (pH 2.0 and concentration always the same, i.e., $2 \times 10^{-2} \text{ mol L}^{-1}$), the sandwich

complexes $\alpha\beta\text{-Co}_4(\text{P}_2\text{W}_{15})_2$ dissociate. Indeed, this dissociation has been detected by electron paramagnetic resonance spectroscopy where evaporation of Co^{2+} has been observed.²¹ This result seems to contradict the preliminary study of $\alpha\beta\text{-}\beta\beta$ interconversion for the $\alpha\beta\text{-Co}_4(\text{P}_2\text{W}_{15})_2$ complex obtained after the addition of 2 equiv of H_3O^+ to the solution containing $\alpha\beta\text{-Co}_4(\text{P}_2\text{W}_{15})_2$. However, this experiment was conducted in an unbuffered solution, where the pH of the solution is increased during this process, with the final pH being 2.5, a pH where the symmetrical $\beta\beta\text{-Co}_4(\text{P}_2\text{W}_{15})_2$ complex is stable.

Moreover, a different ^{31}P NMR final spectrum [P(2) region; Figure 4B] is obtained. In that case, the evolution is also very fast and the final state is already reached before the end of the first ^{31}P NMR recording. It contains a series of four low-intensity signals between 0 and 4 ppm, which might be again attributed to the different isomers of $\text{Na}_2\text{Co}_2(\text{P}_2\text{W}_{15})_2$. In addition, five more intense ^{31}P NMR signals are observed between -5.0 and +23.0 ppm: (i) the major peak at 7.8 ppm is assigned to the compound $\beta\beta\text{-Co}_4(\text{P}_2\text{W}_{15})_2$, (ii) the first pair of

Scheme 3. Proposed Equilibrium between $\beta\beta\text{-Co}_4(\text{P}_2\text{W}_{15})_2$, $\alpha\beta\text{-}\beta\beta$, and $\alpha\alpha\text{-NaCo}_3(\text{P}_2\text{W}_{15})_2$ and Isomers of $\text{Na}_2\text{Co}_2(\text{P}_2\text{W}_{15})_2$

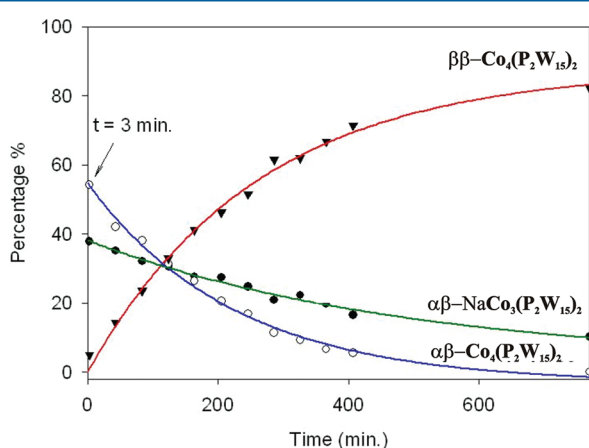
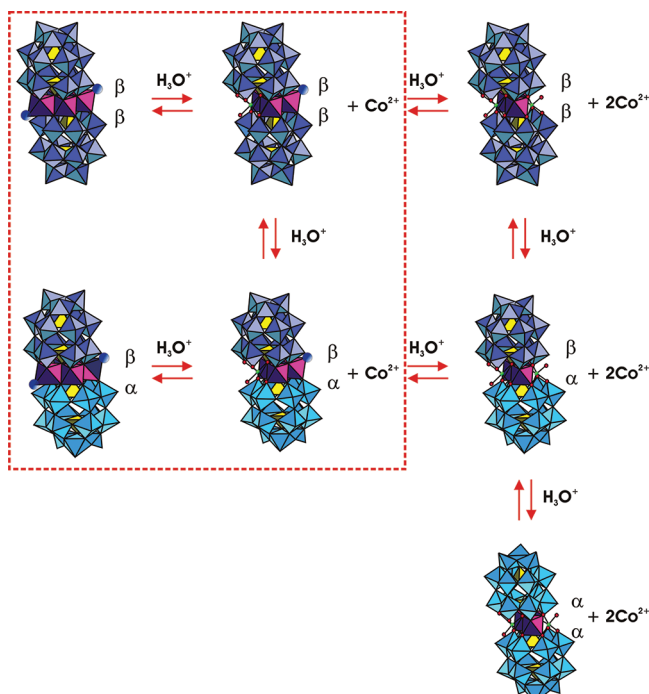


Figure 2. Kinetic study at the low-frequency part [P(2) region] of the 121.5 MHz ^{31}P NMR spectra of the formation of $\beta\beta\text{-Co}_4(\text{P}_2\text{W}_{15})_2$ from $\alpha\beta\text{-Co}_4(\text{P}_2\text{W}_{15})_2$ in $\text{D}_2\text{O}/\text{H}_2\text{O}$ (1:1) in $0.5 \text{ mol L}^{-1} \text{Na}_2\text{SO}_4 + \text{H}_2\text{SO}_4$ (pH 3.0). $c = 2 \times 10^{-2} \text{ mol L}^{-1}$. $T = 300 \text{ K}$. Plot of the percentage of $\alpha\beta\text{-Co}_4(\text{P}_2\text{W}_{15})_2$, $\beta\beta\text{-Co}_4(\text{P}_2\text{W}_{15})_2$ and $\alpha\beta\text{-NaCo}_3(\text{P}_2\text{W}_{15})_2$ versus time (min). The symbols \blacktriangledown indicate signals belonging to $\beta\beta\text{-Co}_4(\text{P}_2\text{W}_{15})_2$; ● correspond to $\alpha\beta\text{-NaCo}_3(\text{P}_2\text{W}_{15})_2$, and ○ to $\alpha\beta\text{-Co}_4(\text{P}_2\text{W}_{15})_2$.

signals, at -4.9 and $+23.0$ ppm, corresponds to $\alpha\beta\text{-NaCo}_3(\text{P}_2\text{W}_{15})_2$ (see Table 1),¹⁰ and (iii) the second pair, at -2.0 and $+16.5$ ppm, should be attributed to a new dissymmetrical compound because $\beta\beta\text{-NaCo}_3(\text{P}_2\text{W}_{15})_2$ [indeed $\alpha\beta\text{-Co}_4(\text{P}_2\text{W}_{15})_2$ seems absent because two peaks at $+10.0$ and $+14.5$ ppm should be present in this case; see Table 1] is absent from this mixture. Thus, these signals might be assigned to the monolacunary species $\beta\beta\text{-NaCo}_3(\text{P}_2\text{W}_{15})_2$ (see Scheme 3).

For $\beta\beta\text{-Co}_4(\text{P}_2\text{W}_{15})_2$, evolution toward a similar distribution of saturated mono- and bilacunary species is also observed.

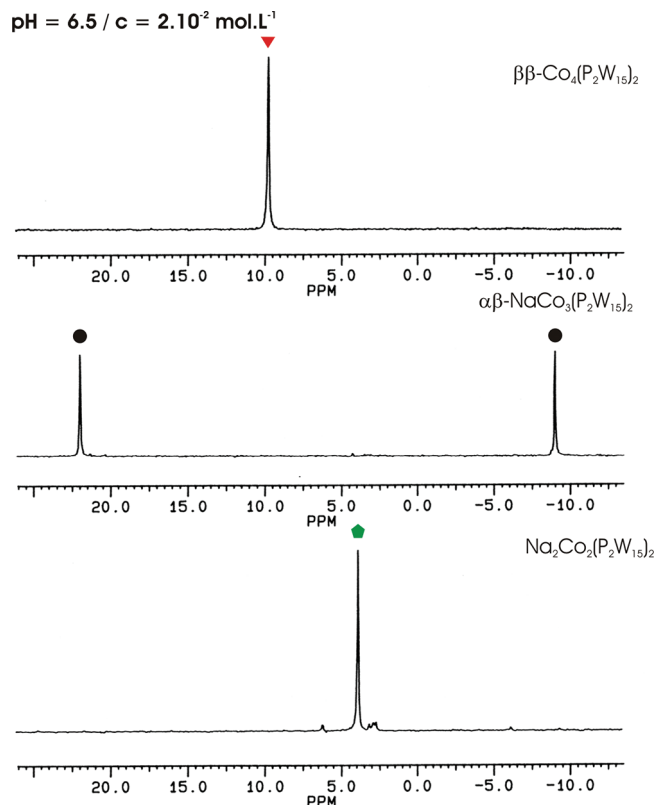


Figure 3. Low-frequency [part P(2) region] 121.5 MHz ^{31}P NMR spectra of $\beta\beta\text{-Co}_4(\text{P}_2\text{W}_{15})_2$, $\alpha\beta\text{-NaCo}_3(\text{P}_2\text{W}_{15})_2$, and $\text{Na}_2\text{Co}_2(\text{P}_2\text{W}_{15})_2$ ($t = 0$); $c = 2 \times 10^{-2} \text{ mol L}^{-1}$ of $0.5 \text{ mol L}^{-1} \text{Na}_2\text{SO}_4$ (pH 6.5)/ D_2O (2:1). $T = 300 \text{ K}$.

Effect of the Concentration on the $\alpha\beta\text{-}\beta\beta$ Interconversion. However, a different behavior is observed for $\alpha\beta\text{-Co}_4(\text{P}_2\text{W}_{15})_2$ in a diluted solution ($0.5 \times 10^{-4} \text{ mol L}^{-1}$) and also at relatively low pH (pH < 3.5; Figure 4C). In such a diluted solution, new species are identified, but neither the saturated symmetric $\beta\beta\text{-Co}_4(\text{P}_2\text{W}_{15})_2$ nor the unsaturated $\alpha\beta\text{-NaCo}_3(\text{P}_2\text{W}_{15})_2$ is observed.

The kinetics of the evolution is very fast because the reaction is already completed before the end of acquisition of the first ^{31}P NMR spectrum (ca. 5 min). It consists [P(2) region] of a series of four peaks between 0 and 4 ppm (Figure 4C).

In similar experimental conditions (pH and concentration), the same spectrum is obtained, whatever the nature of the starting cobalt sandwich complex, i.e., $\beta\beta\text{-Co}_4(\text{P}_2\text{W}_{15})_2$, $\alpha\beta\text{-NaCo}_3(\text{P}_2\text{W}_{15})_2$, and $\alpha\alpha\text{-Na}_2\text{Co}_2(\text{P}_2\text{W}_{15})_2$.

According to the very narrow range of P(2) chemical shifts, the four signals likely belong to dinuclear cobalt sandwich complexes obtained after the evaporation of one [from $\text{NaCo}_3(\text{P}_2\text{W}_{15})_2$] or two [from $\text{Co}_4(\text{P}_2\text{W}_{15})_2$] external Co atoms. These peaks may be attributed to the mixture of $\alpha\alpha$, $\beta\beta$, and $\alpha\beta$ isomers of $\text{Na}_2\text{Co}_2(\text{P}_2\text{W}_{15})_2$, where the two first isomers ($\alpha\alpha$ and $\beta\beta$) are symmetrical (one signal each), whereas the last one ($\alpha\beta$) is dissymmetrical and should present two signals.

According to these results, in a diluted solution and an acidic medium (pH < 3.5), $\alpha\beta\text{-Co}_4(\text{P}_2\text{W}_{15})_2$ likely evolves to a monolacunary species $\alpha\beta\text{-NaCo}_3(\text{P}_2\text{W}_{15})_2$ by evaporation of an external Co atom; this first step is followed immediately by the departure of the second external Co atom. The resulting bilacunary species $\alpha\beta\text{-Na}_2\text{Co}_2(\text{P}_2\text{W}_{15})_2$ then isomerizes partially to $\alpha\alpha\text{-Na}_2\text{Co}_2(\text{P}_2\text{W}_{15})_2$ and $\beta\beta\text{-Na}_2\text{Co}_2(\text{P}_2\text{W}_{15})_2$. The three

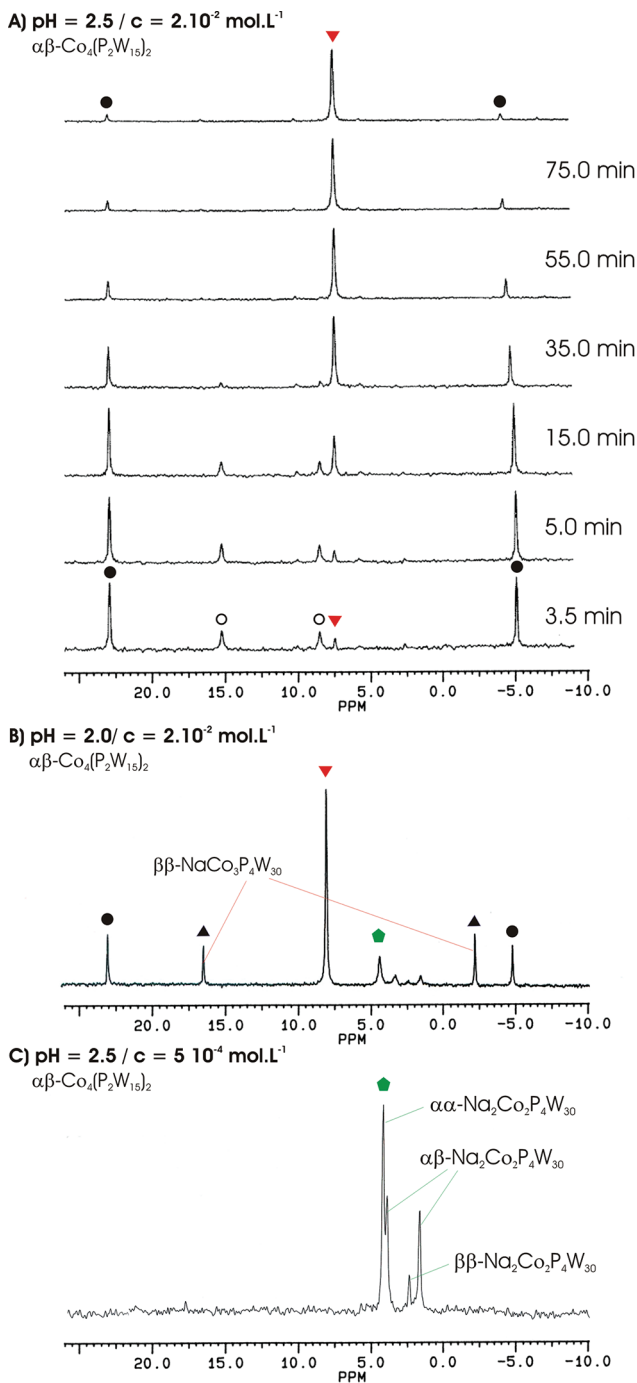


Figure 4. Low-frequency [part P(2) region] 121.5 MHz ^{31}P NMR spectra of $\alpha\beta\text{-Co}_4(\text{P}_2\text{W}_{15})_2$. $T = 300\text{ K}$. Evolution at (A) pH 2.5 and $c = 2 \times 10^{-2} \text{ mol L}^{-1}$, (B) pH 2.0 and $c = 2 \times 10^{-2} \text{ mol L}^{-1}$, and (C) pH 2.5 and $c = 5 \times 10^{-4} \text{ mol L}^{-1}$.

isomers stay in equilibrium (Scheme 3). In the case of $\beta\beta\text{-Co}_4(\text{P}_2\text{W}_{15})_2$, the first step should lead to $\beta\beta\text{-NaCo}_3(\text{P}_2\text{W}_{15})_2$, which evolves similarly to the same mixture of $\text{Na}_2\text{Co}_2(\text{P}_2\text{W}_{15})_2$ through both $\beta\beta\text{-NaCo}_3(\text{P}_2\text{W}_{15})_2$ and/or $\alpha\beta\text{-NaCo}_3(\text{P}_2\text{W}_{15})_2$. Thus, both the concentration of the polyoxometalate and the pH of the solution are crucial parameters for the stability and interconversion of cobalt sandwich compounds. All of the results suggest that, at pH < 3.5, tetracobalt species first lose one external Co atom to form a monolacunary complex $\text{NaCo}_3(\text{P}_2\text{W}_{15})_2$. Second, depending on the concentration, the monolacunary complex $\text{NaCo}_3(\text{P}_2\text{W}_{15})_2$ can be isomerized and

react with Co^{2+} to give back the saturated complex ($\alpha\beta\text{-}\beta\beta$ interconversion) or could lose a second Co atom to form the bilacunary species $\text{Na}_2\text{Co}_2(\text{P}_2\text{W}_{15})_2$ (Scheme 3).

Kinetic Study Followed by Electrochemistry. We have already shown that both $\beta\beta\text{-Co}_4(\text{P}_2\text{W}_{15})_2$ and $\alpha\beta\text{-Co}_4(\text{P}_2\text{W}_{15})_2$ are stable in an aqueous solution in the range $3.5 \leq \text{pH} \leq 7.5$ whatever the concentration ($\geq 0.5 \text{ mmol L}^{-1}$).¹⁷ At these concentrations, symmetrical $\beta\beta\text{-Co}_4(\text{P}_2\text{W}_{15})_2$ presents three processes of reduction between -0.30 and -0.95 V versus saturated calomel electrode (SCE) corresponding to the reduction of W ($\text{W}^{\text{VI}}/\text{W}^{\text{V}}$). These three processes are reversible and involve four electrons each. The third wave is split by 85 mV (Table 2); this splitting is more easily detected in differential pulse voltammetry (DPV). In the case of the dissymmetrical $\alpha\beta\text{-Co}_4(\text{P}_2\text{W}_{15})_2$, we still observe three processes of reduction, but the waves are broader (Figure 5).

However, a different behavior is observed at pH < 3.5, where interconversion and decomplexation processes are observed. While in the case of $\beta\beta\text{-Co}_4(\text{P}_2\text{W}_{15})_2$ evolution is relatively slow, for $\alpha\beta\text{-Co}_4(\text{P}_2\text{W}_{15})_2$, the first state is already reached during the preparation of the solution.

Figure 6 presents the evolution with time of the cyclic voltammetry (CV) and DPV of $\beta\beta\text{-Co}_4(\text{P}_2\text{W}_{15})_2$ in an aqueous solution (pH 2.5 and $c = 5 \times 10^{-4} \text{ mol L}^{-1}$). In the initial state, $\beta\beta\text{-Co}_4(\text{P}_2\text{W}_{15})_2$ presents also three processes of reduction between -0.30 and -0.95 V corresponding to the reduction of W ($\text{W}^{\text{VI}}/\text{W}^{\text{V}}$). These three processes are still reversible and also involve four electrons per process, and the third wave is again split, by ca 50 mV (Table 2).

The change with time (in the range 0–60 min) of the CV curves at pH 2.5 and $c = 5 \times 10^{-4} \text{ mol L}^{-1}$ shows the presence of several “isovoltamperometric” points (analogue to isosbestic points in UV-visible absorption spectroscopy). These results suggest evolution of the initial compound to the final ones without significant concentration of any transient species.

During evolution, the first reduction process is split into two bielectronic reversible waves. At the level of the second reduction process, we also note the vanishing of the initial wave of reduction at -0.636 V for the benefit of a new wave at -0.544 V . Finally, we do not notice any change for the third process of reduction (Figure 6A).

Evolution with time of the DPV curves in the same conditions of concentrations and pH shows again the presence of two isovoltamperometric points. At the level of the second reduction process, we observe the progressive decrease of a peak at -0.504 V and the increase of a new peak at -0.590 V . The corresponding kinetic data are represented in Figure 6C,D: the peak currents Δi measured at -0.504 and -0.590 V are plotted versus time. We observe simultaneously an exponential decrease of Δi measured at -0.504 V as well as an exponential growth of Δi measured at -0.590 V . The plot of $\pm \ln\{[\Delta i(t) - \Delta i(\infty)]/[\Delta i(0) - \Delta i(\infty)]\}$ versus time agrees with a pseudo-first-order reaction for both potentials (Figure 6D).

From these plots, the apparent kinetic constant may be easily obtained, namely, $k_{\text{app}}^+ = 0.071 \pm 0.009 \text{ min}^{-1}$ (at -0.504 V) and $k_{\text{app}}^- = 0.062 \pm 0.009 \text{ min}^{-1}$ (at -0.590 V). Lowering the pH leads to the reaction proceeding faster (Table 3).

Kinetic Study Followed by UV-Visible Spectroscopy. To confirm these results, a kinetic study in the same conditions (i.e., concentration and pH) was conducted by UV-visible spectroscopy also from $\beta\beta\text{-Co}_4(\text{P}_2\text{W}_{15})_2$.

Table 2. Electrochemical Data at pH 3.5 and 2.5 of the Tetra-, Tri-, and Dinuclear Dawson-Derived Sandwich Complexes^a

compound	pH 2.5			pH 3.5		
	W(1)	W(2)	W(3)	W(1)	W(2)	W(3)
$\beta\beta\text{-Co}_4(\text{P}_2\text{W}_{15})_2$	-0.365 (4e, 53)	-0.556 (4e, 160)	-0.785 (2e, 72) -0.835 (2e, 91)	-0.436 (4e, 71)	-0.641 (4e, 144)	-0.832 (2e, 64) -0.917 (2e, 94)
$\alpha\beta\text{-Co}_4(\text{P}_2\text{W}_{15})_2$	-0.354 (2e, 60) ^b -0.416 (2e, 66) ^b	-0.534 (4e, 80) ^b -0.532 (4e, 76) ^b	-0.788 (2e, 74) ^b -0.837 (2e, 94) ^b	-0.467 (4e, 126)	-0.673 (4e, 114)	-0.903 (4e, 100)
$\alpha\beta\text{-NaCo}_3(\text{P}_2\text{W}_{15})_2$	-0.349 (2e, 47) ^b -0.406 (2e, 61) ^b	-0.537 (4e, 82) ^b -0.532 (4e, 76) ^b	-0.760 (2e, 89) ^b -0.831 (2e, 73) ^b	-0.470 (2e, 93)	-0.660 (4e, 83)	-0.835 (4e, 65)
$\text{Na}_2\text{Co}_2(\text{P}_2\text{W}_{15})_2$	-0.348 (2e, 44) -0.408 (2e, 56)	-0.529 (4e, 81)	-0.759 (2e, 94) -0.833 (2e, 71)			

^aAll redox potentials E° , approximated by $(E_p^+ + E_p^-)/2$ for the reversible steps, are given in V versus SCE as obtained from cyclic voltammetry ($v = 20 \text{ mV s}^{-1}$) in 0.5 M $\text{Na}_2\text{SO}_4 + \text{H}_2\text{SO}_4$. Glassy carbon electrode. Under bracket: (number of electrons n ; ΔE_p is the peak splitting). ^bThe potentials correspond to the evolved solution, where the kinetic of evolution is too rapid at pH < 3.5 for $\alpha\beta\text{-Co}_4(\text{P}_2\text{W}_{15})_2$, $\alpha\beta\text{-NaCo}_3(\text{P}_2\text{W}_{15})_2$, and $\text{Na}_2\text{Co}_2(\text{P}_2\text{W}_{15})_2$, $c = 5 \times 10^{-4} \text{ mol L}^{-1}$.

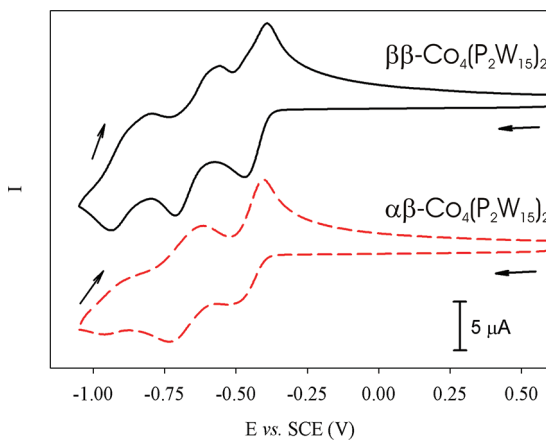


Figure 5. Cyclic voltammograms of $5 \times 10^{-4} \text{ mol L}^{-1} \beta\beta\text{-Co}_4(\text{P}_2\text{W}_{15})_2$ and $\alpha\beta\text{-Co}_4(\text{P}_2\text{W}_{15})_2$ in $0.5 \text{ mol L}^{-1} \text{Na}_2\text{SO}_4 + \text{H}_2\text{SO}_4$ (pH 3.5). Scan rate: 20 mV s^{-1} .

We observe a significant variation of the absorbance versus time with a hypsochromic shift of the maximum of absorbance (Figure 7A).

Analysis of the kinetic data was performed at $\lambda = 600$ and 536 nm. The plot of $[A(t) - A(\infty)]$ versus time shows respectively an exponential decrease and increase of the absorbance. The logarithmic treatment $\pm \ln\{[A(t) - A(\infty)]/[A(0) - A(\infty)]\} = f(t)$ (Figure 7B) agrees also with a pseudo-first-order reaction, allowing one to measure the apparent kinetic constants k_{app}^- and k_{app}^+ .

The measured values are in agreement to those obtained by electrochemistry, with $k_{\text{app}}^+ = 0.069 \pm 0.013 \text{ min}^{-1}$ and $k_{\text{app}}^- = 0.056 \pm 0.013 \text{ min}^{-1}$ at pH 2.5. Varying the pH shows that the reaction is more rapid at lower pH, which is in agreement with the electrochemical study (Table 3).

According to the NMR data, at these low concentrations, the final species is $\text{Na}_2\text{Co}_2(\text{P}_2\text{W}_{15})_2$ (mixture of isomers; see above). Thus, when $\text{Co}_4(\text{P}_2\text{W}_{15})_2$ is less concentrated than H_3O^+ , we observe decomplexation of the external Co^{2+} cations. Consequently, the $[\text{H}_3\text{O}^+]/[\text{Co}_4(\text{P}_2\text{W}_{15})_2]$ ratio plays a paramount role for the complexation/decomplexation process (see Table 3). These results agree with a series of successive equilibria, allowing one to pass from saturated compound $\text{Co}_4(\text{P}_2\text{W}_{15})_2$ to mono- and bilacunary complexes $\text{Na}_1\text{Co}_3(\text{P}_2\text{W}_{15})_2$ and $\text{Na}_2\text{Co}_2(\text{P}_2\text{W}_{15})_2$ (see Scheme 3).

CONCLUSION

In this work, we first report interconversion between $\alpha\beta\text{-Co}_4(\text{P}_2\text{W}_{15})_2$ and $\beta\beta\text{-Co}_4(\text{P}_2\text{W}_{15})_2$ at pH < 3.5 and a concentration of $2 \times 10^{-2} \text{ mol L}^{-1}$, where only the $\text{NaCo}_3(\text{P}_2\text{W}_{15})_2$ intermediate have been observed by ^{31}P NMR spectroscopy.

At pH < 3.5 and in diluted solution ($c = 0.5 \times 10^{-4} \text{ mol L}^{-1}$), a decomplexation process of $\text{Co}_4(\text{P}_2\text{W}_{15})_2$ leads to the formation of isomers of $\text{NaCo}_3(\text{P}_2\text{W}_{15})_2$ and $\text{Na}_2\text{Co}_2(\text{P}_2\text{W}_{15})_2$. This process has been followed at various pH values by electrochemistry, UV-visible spectroscopy, and ^{31}P NMR spectroscopy. Kinetic parameters are extracted from the electrochemistry and UV-visible experiments and are similar according to accuracy. The kinetic constant of cobalt eviction increases with decreasing pH.

As a result, it appears that both the pH and concentration of H_3O^+ and $\text{Co}_4(\text{P}_2\text{W}_{15})_2$ are of paramount importance in determining the direction of the reaction: when $\text{Co}_4(\text{P}_2\text{W}_{15})_2$ is less concentrated than H_3O^+ , decomplexation of the external Co^{2+} cations is observed, while at $2.5 < \text{pH} < 3.5$ and a high concentration of the unsymmetrical tetracobalt Dawson sandwich complex, only interconversion between $\alpha\beta\text{-Co}_4(\text{P}_2\text{W}_{15})_2$ and $\beta\beta\text{-Co}_4(\text{P}_2\text{W}_{15})_2$ is observed.

These results agree with the presence of successive equilibria between saturated compound $\text{Co}_4\text{P}_4\text{W}_{30}$ and mono- and bilacunary complexes.

EXPERIMENTAL SECTION

General Comment. Most of the common laboratory chemicals were reagent-grade, were purchased from commercial sources, and were used without further purification.

Preparation of the Compounds. The potassium salt of $\alpha\text{-}[P_2W_{18}O_{62}]^{6-}$ and the sodium salt of $\alpha\text{-}[P_2W_{15}O_{56}]^{12-}$ were prepared by published methods.²²

$\beta\beta\text{-Na}_{16}[\text{Co}_4(\text{H}_2\text{O})_2(\text{P}_2\text{W}_{15}\text{O}_{56})_2] \cdot 6\text{H}_2\text{O}$, $\alpha\beta\text{-Na}_{16}[\text{Co}_4(\text{H}_2\text{O})_2(\text{P}_2\text{W}_{15}\text{O}_{56})_2] \cdot 5\text{H}_2\text{O} \cdot 2\text{NaCl}$, $\text{Na}_{18}[\text{Na}_2\text{Co}_2(\text{P}_2\text{W}_{15}\text{O}_{56})_2] \cdot 5\text{H}_2\text{O}$ (1), and $\text{Na}_{12}[\text{NaCo}_3(\text{P}_2\text{W}_{15}\text{O}_{56})_2] \cdot 48\text{H}_2\text{O}$ (2). These complexes were obtained as previously described.^{10,18,19}

NMR. ^{31}P NMR spectra were recorded in 5-mm-o.d. tubes on a Bruker AC 300 apparatus operating at 121.5 MHz in Fourier transform mode (equipped with a QNP probe for ^{31}P NMR). The ^{31}P chemical shifts were measured at 300 K on $2 \times 10^{-2} \text{ mol L}^{-1}$ solutions of the polyanions in aqueous $\text{D}_2\text{O}/\text{H}_2\text{O}$ (1:2) in a 0.5 mol L^{-1} $\text{Na}_2\text{SO}_4/\text{H}_2\text{SO}_4$ solution and were referenced to external 85% H_3PO_4 .

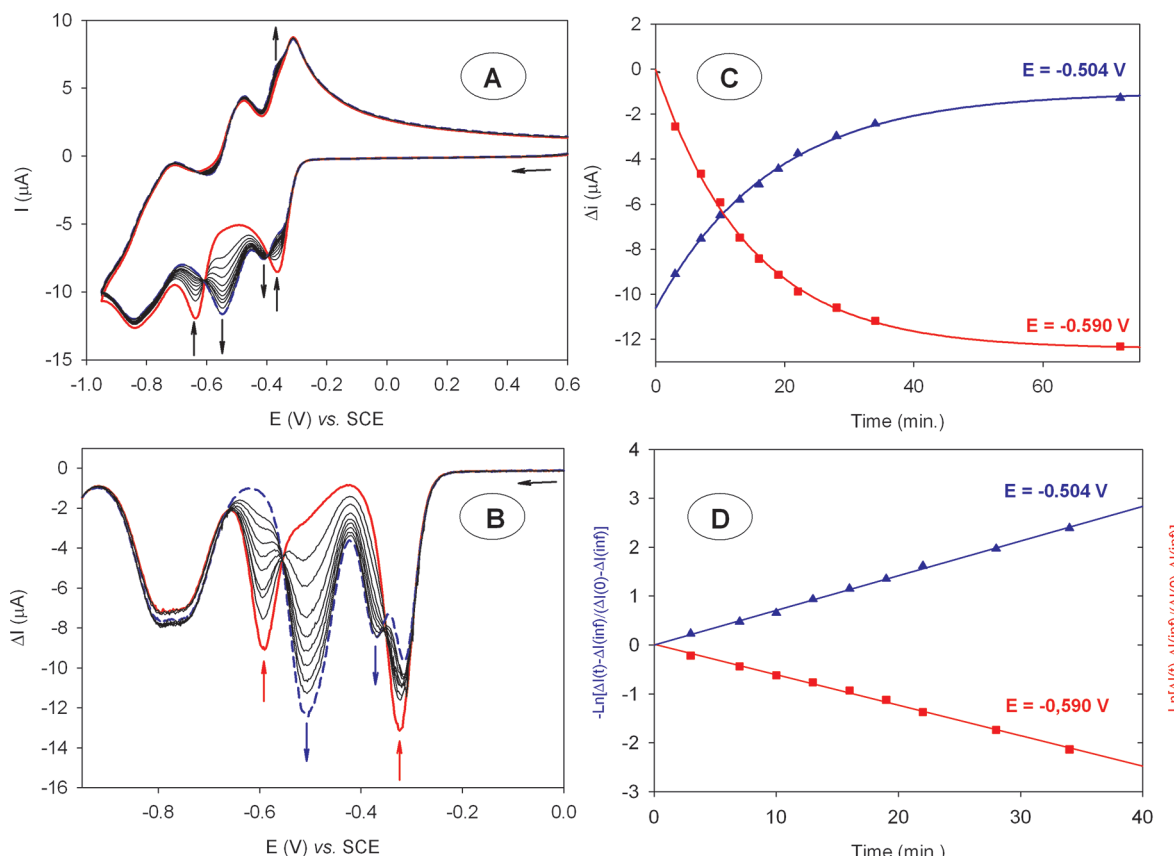


Figure 6. Evolution with time of (A) the CV (scan rate 20 mV s⁻¹) and (B) the DPV (scan rate 25 mV s⁻¹) of 5 × 10⁻⁴ mol L⁻¹ ββ-Co₄(P₂W₁₅)₂ in 0.5 mol L⁻¹ Na₂SO₄ + H₂SO₄ (pH 2.5). Glassy carbon electrode ϕ = 3 mm. (C) Plot of the cathodic peak current Δi_{pc} measured at -0.504 and -0.590 V versus SCE and obtained from the DPV mode versus time (min.). (D) Plots of $+ln\{[\Delta i(t) - \Delta i(\infty)]/[\Delta i(0) - \Delta i(\infty)]\}$ (red line) and of $-ln\{[\Delta i(t) - \Delta i(\infty)]/[\Delta i(0) - \Delta i(\infty)]\}$ (blue line) versus time (min.). Δi_{pc} measured respectively at -0.590 and -0.504 V versus SCE and obtained from the DPV mode versus time (min.). For more clarity, because similar slopes are observed at -0.590 and -0.504 V versus SCE, $-ln\{[\Delta i(t) - \Delta i(\infty)]/[\Delta i(0) - \Delta i(\infty)]\}$ versus time (min.) is plotted for -0.504 V (blue line).

Table 3. Pseudo-First-Order Kinetic Constants for Evolution of ββ-Co₄(P₂W₁₅)₂ Determined from the Electrochemical and UV–Visible Data

pH	$[H_3O^+]/[POM]^a$	complex	k_{app}^- (min ⁻¹)			k_{app}^+ (min ⁻¹)		
			UV-visible	electrochemistry	UV-visible	electrochemistry		
3.50	0.6	ββ-Co ₄ (P ₂ W ₁₅) ₂						
3.00	2.0	ββ-Co ₄ (P ₂ W ₁₅) ₂	0.036 (± 0.013) ($\lambda = 590$ nm)	0.034 (± 0.008) ($E = -0.632$ V)	0.049 (± 0.013) ($\lambda = 550$ nm)	0.042 (± 0.008) ($E = -0.484$ V)		
2.50	6.3	ββ-Co ₄ (P ₂ W ₁₅) ₂	0.056 (± 0.013) ($\lambda = 600$ nm)	0.062 (± 0.009) ($E = -0.590$ V)	0.069 (± 0.013) ($\lambda = 536$ nm)	0.071 (± 0.009) ($E = -0.504$ V)		
2.00	20.0	ββ-Co ₄ (P ₂ W ₁₅) ₂	0.297 (± 0.010) ($\lambda = 610$ nm)	0.275 (± 0.032) ($E = -0.576$ V)	b	0.307 (± 0.010) ($E = -0.436$ V)		

^a[POM] = 5 × 10⁻⁴ mol L⁻¹. ^bThe absence of isosbestic points was noted. We observed only a decrease of the intensity of the absorbance, which does not allow us to calculate the apparent constant of appearance. Only the kinetic constant of disappearance of ββ-Co₄(P₂W₁₅)₂ can be obtained.

446 H₃PO₄ (IUPAC convention) by the substitution method. Optical
447 absorption spectra were recorded with a Shimadzu UV 2101 PC
448 spectrophotometer.

449 **Electrochemical Experiments.** Water used for all electrochemical
450 measurements was obtained by passing through a Milli-RO₄ unit and
451 subsequently through a Millipore Q water purification set. H₂SO₄
452 solutions and solid Na₂SO₄ were commercial products (Prolabo). The
453 electrolyte was made up from a 0.5 mol L⁻¹ Na₂SO₄ aqueous solution,
454 and its pH was precisely adjusted to 2.5 by the addition of a 0.5 mol
455 L⁻¹ H₂SO₄ + Na₂SO₄ aqueous solution. Other pH values were
456 adjusted by the addition of either H₂SO₄ or NaOH (Prolabo). The
457 solutions were deaerated thoroughly for at least 30 min by bubbling

with argon (Ar-U from Air Liquide) and kept under an argon atmosphere during the whole experiment. 458

459 The glassy carbon samples had a diameter of 3 mm. The 460 electrochemical setup was an EG&G 273A instrument driven by a 461 PC with 270 software. Potentials are quoted against a SCE. The 462 counter electrode was a platinum gauze of large surface area. All 463 voltammetric experiments were carried out at room temperature. 464

465 In DPV, current measurements are recorded prior to the pulse and 466 at the end of the pulse. The difference between the two current 467 measurements versus the applied potential results in a differential pulse 468 voltammogram with a peak-shape response. The half-wave potential is 469 calculated using the peak potential value, E_p (eq 1). 469

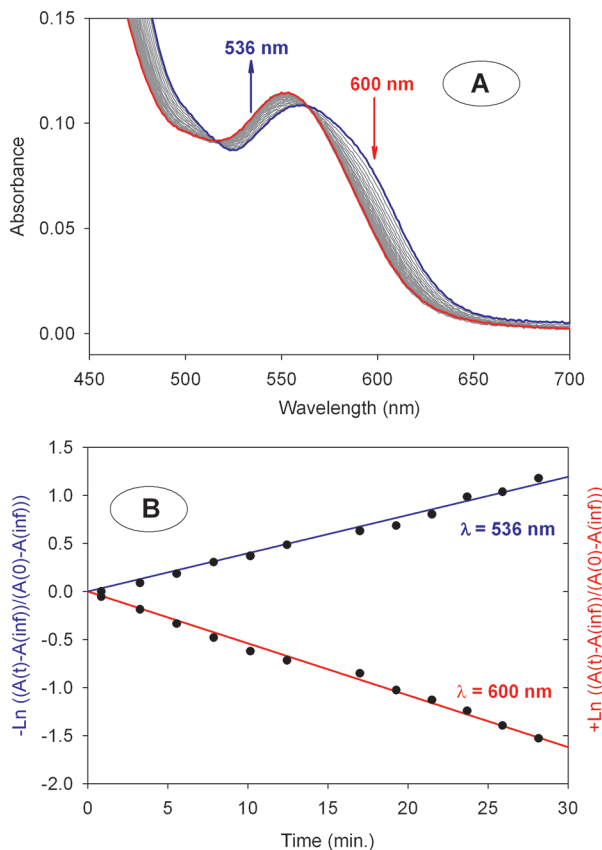


Figure 7. (A) Evolution of $\beta\beta\text{-Co}_4(\text{P}_2\text{W}_{15})_2$ followed by UV-visible spectroscopy. (B) Plots of $+ \ln \{ [A(t) - A(\infty)] / [A(0) - A(\infty)] \}$ (red line) and $- \ln \{ [A(t) - A(\infty)] / [A(0) - A(\infty)] \}$ (blue line) versus time at $\lambda = 600$ and 536 nm, respectively. For more clarity, because similar slopes are observed at -0.590 and -0.504 V versus SCE, $- \ln \{ [A(t) - A(\infty)] / [A(0) - A(\infty)] \}$ versus time (min) is plotted for $\lambda = 536$ nm (blue line). $0.5 \text{ mmol L}^{-1} \beta\beta\text{-Co}_4\text{P}_4\text{W}_{30}$ in $0.5 \text{ mol L}^{-1} \text{Na}_2\text{SO}_4/\text{H}_2\text{SO}_4$ at pH 2.5.

$$E_{1/2} = E_p \pm \Delta E_p / 2 \quad (1)$$

where E_p is the peak potential (V) and ΔE_p is the pulse amplitude (V).

$$\Delta i = nFAD^{1/2}C(\pi t_p)^{-1/2}(1 - \sigma)(1 + \sigma)^{-1} \quad (2)$$

where Δi is the peak current (A), t_p is the pulse period (s), and σ is the pulse height $= \exp[(nF/RT)(\Delta E_p/2)]$.

The peak width at a value of half of the peak current, $W_{1/2}$, follows eq 3 for a waveform with a small amplitude pulse applied. $W_{1/2}$ has a value of $0.0904/n$ (V) for a reversible process at 25 °C.

$$W_{1/2} = 3.25RT/nF \quad (3)$$

where $W_{1/2}$ is the width of the peak at a current equal to half of the peak current (V).

AUTHOR INFORMATION

Corresponding Author

*E-mail: lruhlmann@unistra.fr (L.R.), rene.thouvenot@upmc.fr (R.T.).

Notes

The authors declare no competing financial interest.

ACKNOWLEDGMENTS

This work was supported by the Centre National de la Recherche Scientifique (CNRS) and by the Universities of Paris-Sud 11 and Pierre et Marie Curie Paris 06. This work was also supported by the Agence Nationale de la Recherche (ANR agency), under Projects JC05_52437 and NCPPOM.

REFERENCES

- (1) Katsoulis, D. E. *Chem. Rev.* **1998**, *98*, 359–387.
- (2) Kozhevnikov, I. V. *Chem. Rev.* **1998**, *98*, 171–198.
- (3) (a) *Polyoxometalates: from Platonic Solids to Anti-Retroviral Activity*; Pope, M. T.; Müller, A., Eds.; Kluwer: Dordrecht, The Netherlands, 1994. (b) Herve, M.; Sinoussi-Barre, F.; Chermann, J. C.; Herve, G.; Jasmin, C. *Biochem. Biophys. Res. Commun.* **1983**, *116*, 222–229. (c) Kim, G.-S.; Judd, D. A.; Hill, C. L.; Schinazi, R. F. *J. Med. Chem.* **1994**, *37*, 816–820. (d) Moskowitz, B. L. *Antimicrob. Agents Chemother.* **1988**, *32*, 1300–1303. (e) Wang, X.; Liu, J.; Pope, M. T. *Dalton Trans.* **2003**, 957–960. (f) Wang, X.; Li, F.; Liu, S.; Pope, M. T. *J. Inorg. Biochem.* **2005**, *99*, 452–457. (g) Rhule, J. T.; Hill, C. L.; Judd, D. A.; Schinazi, R. F. *Chem. Rev.* **1998**, *98*, 327–357. (h) Hasenknopf, B. *Front. Biosci.* **2005**, *10*, 275–287. (i) Mukherjee, H. N. *J. Indian Med. Assoc.* **1965**, *44*, 477–479. (j) Yamase, T. *Mol. Eng.* **1993**, *3*, 506–507.
- (4) (a) Neumann, R.; Lissel, M. *J. Org. Chem.* **1989**, *54*, 4607–4610. (b) Kozhevnikov, I. V. *J. Mol. Catal. A: Chem.* **1997**, *117*, 151–158. (c) Harrup, M. K.; Hill, C. L. *Inorg. Chem.* **1994**, *33*, 5448–5455. (d) Pavlova, S. N.; Kuznetsova, L. I.; Matveev, K. I.; Sazonov, V. A.; Popovskii, V. V.; Zhizhina, E. G.; Fenelonov, V. B.; Gavrilov, V. Y. *Kinet. Katal.* **1987**, *28*, 373–379.
- (5) (a) Hu, C. W.; Hashimoto, M.; Okuhara, T.; Misono, M. *J. Catal.* **1993**, *143*, 437–448. (b) Izumi, Y.; Ogawa, M.; Urabe, K. *Appl. Catal. A* **1995**, *132*, 127–140.
- (6) Costa-Coquelard, C.; Schaming, D.; Lampre, I.; Sorgues, S.; Ruhlmann, L. *Appl. Catal. B* **2008**, *84*, 835.
- (7) Finke, R. G.; Droege, M. W. *Inorg. Chem.* **1983**, *22*, 1006.
- (8) (a) Finke, R. G.; Droege, M. W.; Domaille, P. *J. Inorg. Chem.* **1987**, *26*, 3886. (b) Weakley, T. J. R.; Finke, R. G. *Inorg. Chem.* **1990**, *29*, 1235. (c) Ciabrini, J.-P.; Contant, R. *J. Chem. Res.* **1993**, (S)391–512 (M) 2719. (d) Gómez-Garcia, C. J.; Borrás-Almenar, J. J.; Coronado, E.; Ouahab, L. *Inorg. Chem.* **1994**, *33*, 4016. (e) Finke, R. G.; Weakley, T. J. R. *J. Chem. Crystallogr.* **1994**, *24*, 123. (f) Kirby, J. F.; Baker, L. C. *W. J. Am. Chem. Soc.* **1995**, *117*, 10010. (g) Zhang, X.; Duncan, D. C.; Campana, C. F.; Hill, C. L. *Inorg. Chem.* **1997**, *36*, 4208. (h) Müller, A.; Peter, F.; Pope, M.; Gatteschi, D. *Chem. Rev.* **1998**, *98*, 239.
- (i) Meng, L.; Liu, J. *F. Chem. Res. Chin. Univ.* **1998**, *14*, 1. (j) Liu, S.; Kurth, D. G.; Bredenkötter, B.; Volkmer, D. *J. Am. Chem. Soc.* **2002**, *124*, 12280–12287. (k) Liu, S.; Kurth, D. G.; Bredenkötter, B.; Volkmer, D. *J. Am. Chem. Soc.* **2002**, *124*, 12279–12287.
- (9) Thouvenot, R.; Fournier, M.; Franck, R.; Rocchiccioli-Deltcheff, C. *Inorg. Chem.* **1984**, *23*, 598–605.
- (10) Ruhlmann, L.; Cannay, J.; Contant, R.; Thouvenot, R. *Inorg. Chem.* **2002**, *41*, 3811–3819.
- (11) Clemente-Juan, J. M.; Coronado, E.; Gaita-Arino, A.; Gimenez-Saiz, C.; Guedel, H.-U.; Sieber, A.; Bircher, R.; Mutka, H. *Inorg. Chem.* **2005**, *44*, 3389–3395.
- (12) (a) Mbomekalle, I. M.; Keita, B.; Nadjo, L.; Neiwert, W. A.; Zhang, L.; Hardcastle, K. I.; Hill, C. L.; Anderson, T. M. *Eur. J. Inorg. Chem.* **2003**, 3924–3928. (b) Keita, B.; Mbomekalle, I. M.; Nadjo, L.; Anderson, T. M.; Hill, C. L. *Inorg. Chem.* **2004**, *43*, 3257–3263.
- (c) Anderson, T. M.; Hardcastle, K. I.; Okun, N.; Hill, C. L. *Inorg. Chem.* **2001**, *40*, 6418.
- (13) (a) Preliminary crystallographic data for $\text{Na}_{17}[\text{NaMn}_3(\text{H}_2\text{O})_2(\text{P}_2\text{W}_{15}\text{O}_{56})_2] \cdot 4\text{H}_2\text{O}$: triclinic space group $\overline{P}\bar{I}$ with $a = 12.9979(19) \text{ \AA}$, $b = 15.2232(26) \text{ \AA}$, $c = 22.8211(36) \text{ \AA}$, $\alpha = 88.66(2)^\circ$, $\beta = 75.01(2)^\circ$, $\gamma = 66.114(9)^\circ$, and $V = 3971(1) \text{ \AA}^3$. The $\{\text{NaMn}_3\text{P}_4\text{W}_{30}\}$ presents $\beta\beta$ connectivity. The complete crystallographic report will be published later. (b) Ruhlmann, L.; Costa-

552 Coquelard, C.; Canny, J.; Thouvenot, R. *J. Electroanal. Chem.* **2007**,
553 603, 260–268.

554 (14) Additionally, we have reported earlier an unprecedented
555 trinuclear Dawson sandwich complex with internal lacuna for
556 $[\text{NaNi}_3(\text{H}_2\text{O})_2(\text{P}_2\text{W}_{15}\text{O}_{56})_2]^{17-}$ with $\beta\beta$ connectivity resulting from
557 the fusion of two $\beta\{-\text{Ni}_3\text{P}_2\text{W}_{15}\}$ units. See: Schaming, D.; Canny, J.;
558 Boubekeur, K.; Thouvenot, R.; Ruhlmann, L. *Eur. J. Inorg. Chem.* **2009**,
559 5004–5009.

560 (15) All dimetallic sandwich complexes investigated by X-ray
561 crystallography, namely, $\text{Na}_2\text{M}_2(\text{P}_2\text{W}_{15})_2$ ($\text{M} = \text{Fe}^{\text{III}}, \text{Zn}^{\text{II}}, \text{Ni}^{\text{II}}$), exhibit
562 $\alpha\alpha$ connectivity. The dicobalt derivative should likely be isostructural
563 and will be formulated as $\alpha\alpha\text{-Na}_2\text{Co}_2(\text{P}_2\text{W}_{15})_2$.

564 (16) (a) Anderson, T. M.; Zhang, X.; Hardcastle, K. I.; Hill, C. L.
565 *Inorg. Chem.* **2002**, *41*, 2477. (b) Mbomekalle, I. M.; Cao, R.;
566 Hardcastle, K. I.; Hill, C. L.; Amman, M.; Keita, B.; Nadjo, L.;
567 Anderson, T. M. *C.R. Chimie* **2005**, *8*, 1077–1086.

568 (17) Ruhlmann, L.; Canny, J.; Vaisserman, J.; Thouvenot, R. *J. Chem.*
569 *Soc., Dalton Trans.* **2004**, *5*, 794–800.

570 (18) Ruhlmann, L.; Costa-Coquelard, C.; Canny, J.; Thouvenot, R.
571 *Eur. J. Inorg. Chem.* **2007**, 1493–1500.

572 (19) Ruhlmann, L.; Nadjo, L.; Canny, J.; Thouvenot, R. *Eur. J. Inorg.*
573 *Chem.* **2002**, 975–986.

574 (20) The chemical shifts of $\beta\beta\text{-Co}_4(\text{P}_2\text{W}_{15})_2$ differ slightly from those
575 already published¹⁹ especially for the P(1) signals. This results from
576 different experimental conditions (pH and concentration), which
577 induces different paramagnetic shifts more important for the P(1)
578 nuclei, close to the Co^{II} centers.

579 (21) Ohlin, C. A.; Harley, S. J.; McAlpin, J. G.; Hocking, R. K.;
580 Mercado, B. Q.; Johnson, R. L.; Villa, E. M.; Filder, M. K.; Olmstead,
581 M. M.; Spiccia, L.; Britt, R. D.; Casey, W. H. *Chem.—Eur. J.* **2011**, *17*,
582 4408.

583 (22) (a) Ciabrini, J. P.; Contant, R.; Fruchart, J.-M. *Polyhedron* **1983**,
584 *2*, 1229; (b) Contant, R. *J. P. J. Chem. Res., Synop.* **1977** 222. *J. Chem. Res., Miniprint* **1977**, 2601. (c) Contant, R. *Inorg. Synth.* **1990**,
586 *27*, 104.